Advances in Military Technology
Vol. 16, No. 2, 2021, pp. 333-343
ISSN 1802-2308, eISSN 2533-4123
DOI 10.3849/aimt.01521

Modeling and Simulation on the Rotating Band Engraving Process of 23 mm Projectile

V. Minh Do, X. Son Bui, and V. Huong Nguyen*

Faculty of Weapons, Le Quy Don Technical University, Hanoi, Vietnam

The manuscript was received on 16 July 2021 and was accepted after revision for publication as research paper on 20 December 2021.

Abstract:

Dynamic engraving process of 23 mm projectile was studied using numerical simulation. A finite element model of projectile and barrel during the engraving process was constructed, and the deformation process of the driving band, the displacement parameters of the projectile, the force interaction between the projectile and the barrel were determined. To evaluate the simulation model, a semi-static experiment was carried out on an MTS-810 universal testing machine with a cross-head speed of 20 mm min^{-1}. The simulation results show that the mechanism of the 23 mm projectile rotating band engraving process is the plastic deformation process of the rotating band material, engraving time is 1.12 m s, and the projectile velocity after engraving is 105 m s^{-1}. The simulation results reflect the actual rotating band engraving process, which is very distinct from the assumptions used in the classical ballistic model. This work provides an approach to investigating the interior ballistic processes considering the dynamic engraving of rotating bands.

Keywords:

driving band deformation, movement of the projectile, rotating band, rotating band engraving process, simulation

1 Introduction

The physical processes that occur when rotating band engraving play a crucial role in the ballistics parameters of the preliminary period, as well as in the entire firing process [1]. The rotating band engraving process is a complex nonlinear process with transient, high temperature, intensive impact, high-speed friction, and giant deformation [1-3]. In the basic internal ballistics, the rotating band engraving process is often ignored and taken into account through the shot start pressure (SSP) [4]. However, the SSP value does not fully reflect the influence of the rotating band engraving

* *Corresponding author: Department of Munitions, Le Quy Don Technical University, Hoang Quoc Viet 236, Hanoi, Vietnam. Phone: +84 976 51 93 71, E-mail: h4ta.030588@gmail.com*

process on the displacement characteristics of the projectile in the barrel. The publication of the rotating band engraving process mechanism is limited.

There have been several studies on the rotating band engraving process [5-9], however each work has its limitations and it is unable to apply to all driving band engraving processes of other ammunition.

Andrews [5] discussed the effect of the rotating band engraving process on the stress applied to the 155 mm cannon barrel by the experimental method. The result showed that the load of the driving band applied on the barrel during the engraving process is of great value, which can lead to cracking and destroying the barrel.

Carlucci et al. [6] used sensors to measure the projectile base pressure and the projectile's acceleration during the rotating band engraving process. However, in that study, an inevitable problem was how to calibrate the accelerometer accurately under such high acceleration.

Tao et al. [7] studied the effect of the rotating band engraving process on the maximum pressure with the numbering change of shots in the internal ballistic law through the shot start pressure. However, some kinds of limitations were unavoidable due to the application of analytical formulas to determine the shot start pressure.

Wu et al. [8] studied the interaction between the projectile and the barrel during the rotating band engraving process by experimental methods under semi-static and dynamic loading conditions. Semi-static load conditions were proceeded on a universal testing machine. Dynamic loading conditions were carried out on a gas gun designed by the authors. They concluded that the strain rate has a great influence on the degree of deformation of the driving band during the engraving process.

Sudarsan et al. [9] used the Dimensional Analysis Method to study the rotating band engraving process, and they established an analytical formula to determine the shot start pressure value for the gun system with the rifling barrel. Based on the mathematical model, a dependence of the shot start pressure in the width of the land and the groove of the barrel, the width of the driving band and the barrel diameter is depicted. However, the study has not clarified the mechanism of the rotating band engraving process. The calculation model has not fully reflected the influence of other parameters of the body, rotating band, and barrel on the engraving process.

It is difficult to observe the deformation and the formation of engraved vestiges on the rotating band during the rotating band engraving under actual firing conditions. The engraving process is a complex nonlinear process, so it is very difficult to establish and solve the rotating band engraving problem accurately. The development of modern computational mechanics and computer technology, especially the advent of the finite element method provides an effective way to solve the problem of the rotating band engraving dynamics. Besides, due to the high cost, it is necessary to use numerical simulation methods to study the dynamics of the engraving process. This article uses the ANSYS AUTODYN 3D software to simulate the rotating band engraving process of 23 mm Projectile. Digitizing the dynamics of the rotating band process is important to accurately obtain the changing laws (distance, velocity, acceleration) of the projectile over time. To meet requirements, the load placed on the bottom of the projectile requires high accuracy. It is difficult for the classical ballistic model to accurately calculate this load during the rotating band engraving phase. To ensure the accuracy of the numerical simulation model, this paper proposes to use the experimentally measured projectile base pressure data.

In the article, the characteristics such as deformation, the stress of the driving band, the kinematic characteristics of the projectile during the rotating band engraving

process, and the pressure value of the barrel applied on the rotating band are determined. The numerical simulation results were compared and evaluated with the semi-static compression test results to analyze and clarify the mechanism of the rotating band engraving process.

2 Simulation Model and Material Model

The geometric model of the rotating band engraving process is shown in Fig. 1. The OX is the symmetry axis of the barrel. Ignoring the influence of the binding force between the projectile and the cartridge case, the rotating band was initially in contact with the forcing cone.

The projectile-barrel model used in the numerical simulation is based on the structure of the 23 mm armor-piercing incendiary tracer projectile and the 23 mm anti-aircraft guns ZU-23-2. The 23 mm armor-piercing incendiary tracer projectile consists of body, ballistic cap, incendiary substance, driving band, and tracer (Fig. 2a).

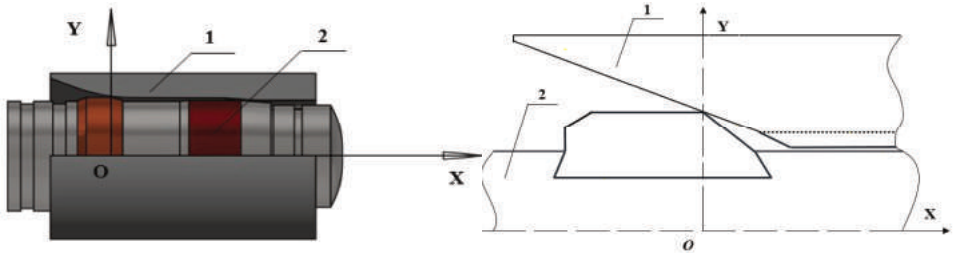

Fig. 1 Geometric model of the rotating band engraving process
1. Truncated barrel; 2. Projectile

To simplify the simulation process, the projectile is simplified to include: body and driving band rigidly linked together. The simplified projectile mass is equal to the real projectile mass. The simplified projectile's geometry model is shown in Fig. 2b.

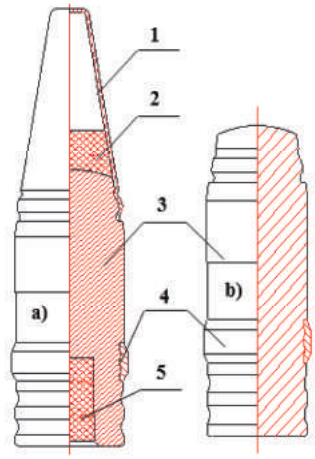

Fig. 2 Construction of 23 mm *Armor-Piercing Incendiary Tracer Projectile a) Real construction; b) Simplified construction 1. Ballistic cap; 2. Incendiary substance; 3. Body; 4. Driving band; 5. Tracer*

The primary geometric parameters of the barrel and projectile used for the numerical simulation model are shown in Fig. 3. The geometrical parameters of the barrel include the width of the land *a*, the width of the groove *b*, the depth of the groove *t*, the smooth forcing cone diameter D_1; the groove diameter D_2; the land diameter D_3; the length of smooth forcing cone H_1; the length of rifling forcing cone H_2; the engraving displacement *H*. The geometrical parameters of the projectile include the diameter of the rotating band D_r; the diameter of aft-end rotating band *D*s; the width of the rotating band *B; α, β* - cone angles.

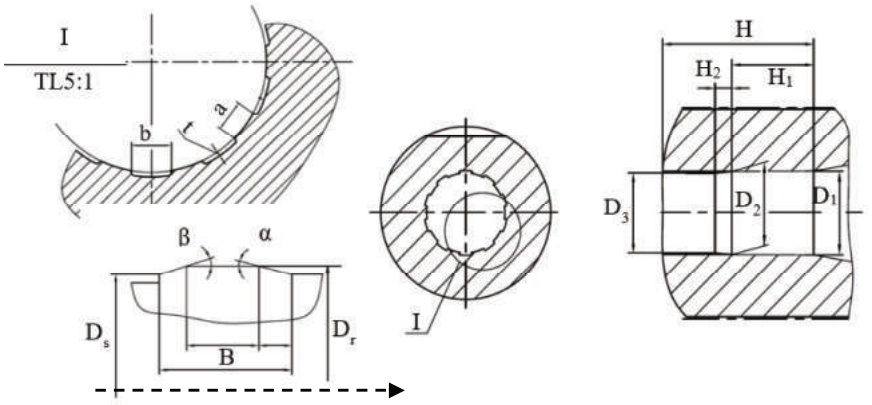

Fig. 3 Primary geometric parameters of barrel and projectile

The dimension values of barrel and rotating band used in the simulation are shown in Tab. 1.

Tab. 1 Dimension values of barrel and rotating band, unit [mm]

D_1	D_2	D_3	H_1	H_2	H	a	b	t	B	D_r	D_s	α	β
24.1	23.9	23	24	5	34	3.2	4	0.45	8.8	24.1	22.9	14°	20.56°

The finite element mesh used for the simulation is shown in Fig 4. Eight-node hexahedral elements are used to build a finite element model. Numerical simulations are performed by ANSYS AUTODYN software. All of the parts were modeled with a Lagrangian mesh composed of deformable elements with a finer discretization in the vicinities of the interface elements. The dimension of elements was approximately 0.5 mm. The whole numerical model consisted of 99 360 elements and 419 693 nodes, among which 4 360 elements were for the rotating band.

In the simulation, the recoil of the barrel was neglected. The front and rear portions of the barrel are fixed to prevent motion. A pressure load is applied on the base of the projectile. The time-base pressure curve of the 23 mm armor-piercing incendiary tracer projectile is determined by test firing, measured with a Piezoelectric Kistler 6 215 Sensor. Fig. 5 shows the time-base pressure curve used in the numerical simulation model.

To simplify the calculation model, while still predicting the behavior of the rotating band and the working mechanism of the driving band during the rotating band engraving process, it is assumed that the cannon barrel and the body during the rotating band engraving process are rigid. Material and material model of the body, rotating band, and barrel are shown in Tab. 2. The material parameters of the body, driving band, and barrel are taken from the AUTODYN software library [10].

The contact eroding nodes to surface algorithm available in AUTODYN were used to model the contact between the rotating band and the inner wall of the barrel. According to [1], the value of the friction coefficient was set to be 0.1.

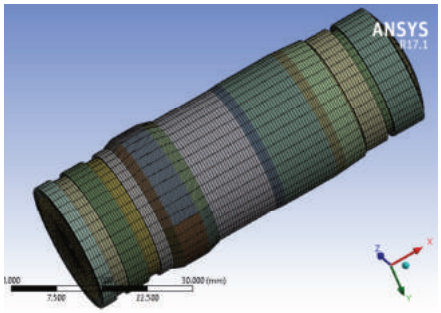

Fig. 4 Mesh of finite element model

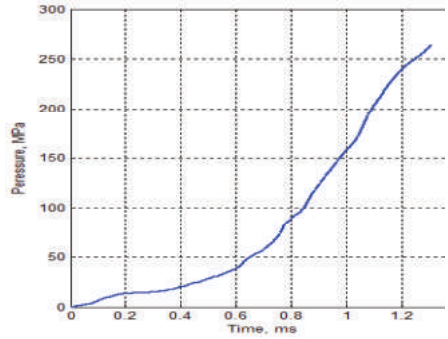

Fig. 5 Time-base pressure curve during rotating band engraving

Tab. 2 Material and material models

Part	Material	Strength Model	Failure Model
Rotating band	CU-OFHC2	Johnson-Cook	Johnson-Cook
Body	Steel	—	—
Barrel	Steel	—	—

3 Experiment

To evaluate the simulation results, a semi-static experiment was carried out on an MTS-Landmark 810 universal testing machine (Fig. 6). The 3 samples of the 23 mm armor piercing incendiary tracer projectile are compressed through the truncated barrel of the 23 mm anti-aircraft guns ZU-23-2 with a cross head speed of 20 mm min^{-1}. After compression, the geometric dimensions of the rotating band were measured.

Fig. 6 Quasi-static engraving of rotating band on MTS-Landmark 810

Some geometric dimensions, such as the width of engraved vestiges and band length under the land portion of the barrel were compared between simulation and semi-static experiment (Figs 7 and 8). The measured dimensions of the rotating band after the engraving process are shown in Tab. 3. The difference in the width of the groove on the rotating band between the experiment (3.29 mm) and the numerical simulation (3.24 mm) is 0.05 (or 1.52 %). The average band length under the land portion of the barrel of the experiment is 10.27 mm, whereas the band length of numerical results is 10.65 mm. The difference of band length under the land portion between the experiment and the numerical simulation average data is 0.38 mm (or 3.57 %).

The quasi-static test does not describe accurately the strain rate of the rotating band material in the actual engraving process. However, the suitability between the results of the experiment and simulation initially shows that the simulation method can be used in analyzing the rotating band engraving process.

4 Analysis and Discussion

In this section, the characteristic parameters for the rotating band engraving process of the 23 mm armor-piercing incendiary tracer projectile will be presented. The simulation results are analyzed to understand clearly the mechanism of the rotating band engraving process.

4.1 Mechanism of Rotating Band Engraving Process When Firing of the 23 mm Armor-Piercing Incendiary Tracer Projectile

Fig. 9 presents the deformation process of the driving band at different times during the rotating band engraving process of the 23 mm projectile.

Tab. 3 Dimensions of engraved vestiges on rotating band [mm]

Experiment		The band length under the land portion of the barrel	Engraved vestiges' width
Experiment	1	10.20	3.28
	2	10.30	3.21
	3	10.30	3.37
	Average	10.27	3.29
Simulation		10.65	3.24

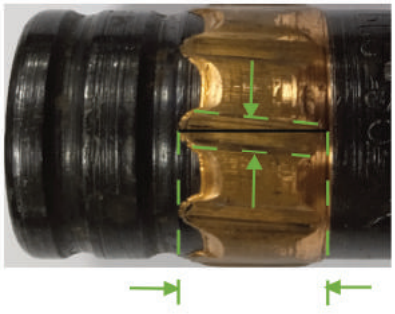

Fig. 7 Deformation of the driving band after quasi -static compression experiment

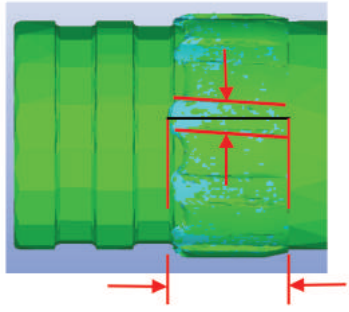

Fig. 8 Deformation of driving band after firing by simulation

The results show that under the increase of the gas pressure, the rotating band is pushed into the barrel and pressed between the body and the barrel. In the rotating band engraving process, the rotating band is extruded by the forcing cone portion, land portion, and groove portion of the barrel. The engraved grooves on the rotating band are formed by the rifling land, the rotating band material is extruded at the end of the formed grooves and does not separate from the rotating band. The accumulation of band material resulting from the extrusion was also apparent at the end of the land portion. However, the length of the rotating band's extension parts under the land, groove portion of the barrel is different.

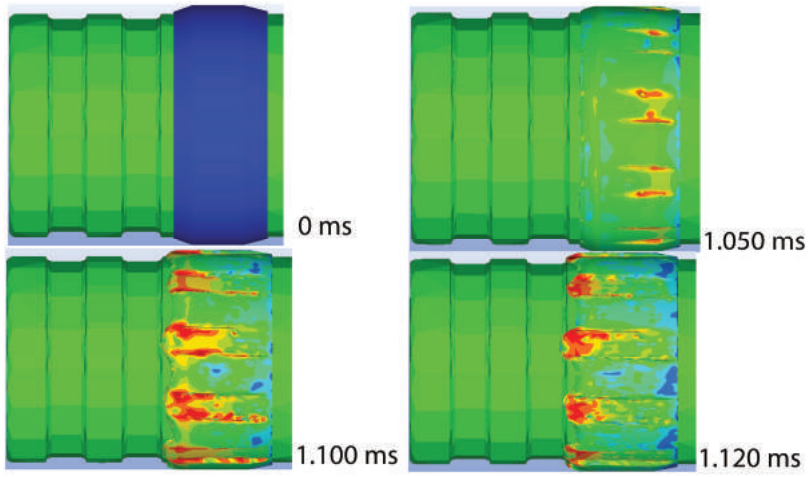

Fig. 9 Morphological deformation of driving band during engraving process

Fig. 10 shows the material state of the driving band during the rotating band engraving process. The results show that the driving band material is totally in the elastic-plastic state, and there is no damage to the band material during the rotating band engraving process.

The mass of the rotating band was measured after the quasi-static test and numerical simulation (Fig. 11). The obtained results show that the mass of the rotating band has not changed. This proves that during the rotating band engraving process, the rotating band material does not break out. This result is consistent with the result on the material state of the rotating band during the engraving process, which is shown in Fig. 10.

The radial displacement of a point on the rotating band surface (under groove portion of the barrel) during the rotating band engraving process is shown in Fig. 12. Fig. 12 shows that during the engraving process, the rotating band is compressed in the radial direction, the radial displacement of the rotating band is almost linear in the engraving travel $0 \div 24$ mm corresponding with the length of smooth forcing cone H_1. The maximum radial displacement (0.1 mm) is achieved when the projectile travels 24 mm (H_1) corresponds to the rotating band redundancy $\delta = (D_r - D_2)/2 = 0.1$ mm. The radial displacement of the point on the driving band surface is almost constant (0.1 mm) corresponding with the length of rifle cone H_2. Then, due to the elastic property, the rotating band material has an opposite radial displacement and compresses the groove surface of the barrel, ensuring gas-tight conditions. The simulation results of the radial displacement are consistent with the original structural parameters of the

rotating band, 23 mm barrel, and accurately reflect the working requirements of the rotating band when firing. These conclusions can somehow demonstrate the validity of simulations in this paper

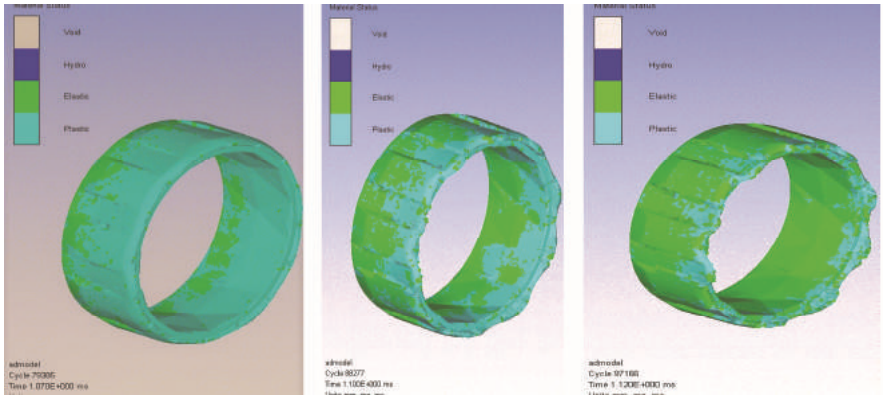

Fig. 10 Material state of the driving band during rotating band engraving process

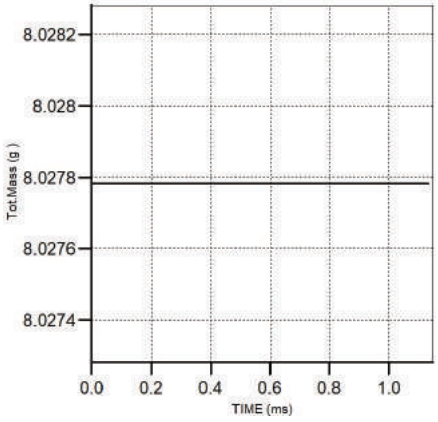

Fig. 11 Change of band mass during the rotating band engraving process

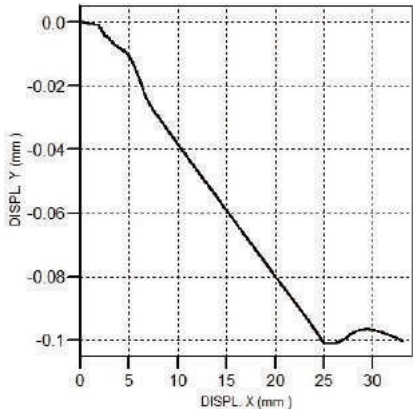

Fig. 12 Radial displacement of a point on the driving band surface

4.2 Movement Parameters of the Projectile During the Rotating Band Engraving Process

Figs 13 and 14 show the projectile displacement-time curve and the projectile velocity-distance curve during the rotating band engraving process.

The velocity-time curve (Fig. 14) clearly shows the two stages of the rotating band engraving process. In the first stage, the projectile moves in a distance of 24 mm. In this period, the rotating band is mainly pressed and extruded by the first cone of the barrel. During this period, the projectile velocity increases rapidly, almost linearly with the engraving distance. At the end of the stage, the projectile reaches a velocity of about 90 m s^{-1}. In the second stage, the rotating band is pushed into the rifling barrel, the engraving vestiges are formed, which are evident on the nearly horizontal segment of the velocity-distance curve. Due to the rapid increase in resistance force, although the base pressure continues to increase, the velocity in this period increases very slow-

ly, almost unchanged. From the velocity graph of the projectile during the rotating band engraving process, it is shown that the projectile velocity is about 105 m s^{-1} at the end of the engraving process. This result is significantly different from the assumption of the classical ballistic theory considering that the rotating band engraving process takes place instantaneously, and the projectile begins to move after the engraving process with a velocity equal to zero.

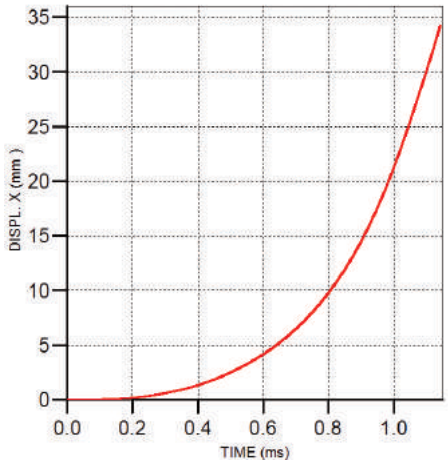

Fig. 13 Displacement-time curve

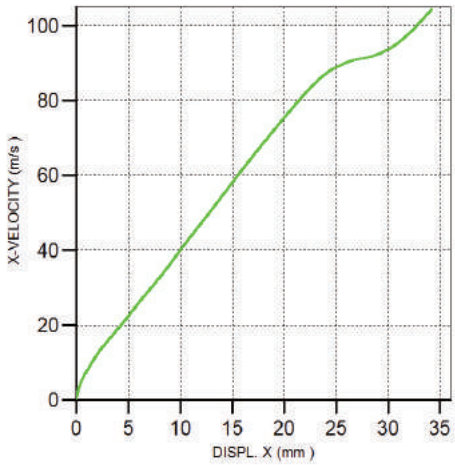

Fig. 14 Velocity-distance curve

Some of the characteristics of the engraving process results of the 23 mm armor piercing incendiary tracer projectile are obtained and shown in Tab. 4.

Tab. 4 Characteristics of the engraving process results of the 23 mm *projectile*

No.	Parameter	Value
1	Displacement of the projectile at the end of the engraving process [mm]	34
2	A time when the driving band is completely engraved into the rifling barrel [ms]	≈ 1.12
3	Velocity of the projectile at the end of the engraving process [m s^{-1}]	≈ 105
4	Projectile base pressure at the time of complete driving band engraving [MPa]	≈ 216
5	Velocity at engraving completion point/Muzzle velocity [%]	10.7
6	Engraving pressure at engraving completion point/Maximum pressure [%]	65.45

Research [11] shows that the velocity of the projectile has reached 10 % of the muzzle velocity and the engraving pressure (projectile base pressure) has reached 65 % of the maximum value when the band engraved in rifling completely. Results of velocity and engraving pressure through numerical analysis are shown in Tab. 4. These conclusions can somehow demonstrate the validity of the simulations in this paper.

4.3 The Pressure of the Barrel Gun on the Driving Band During Rotating Band Engraving

Fig. 15 shows the simulation result about the pressure of the barrel gun on the rotating band during the rotating band engraving process.

The graph has shown that the pressure of the barrel gun on the rotating band changes very complicatedly during the rotating band engraving process. The pressure increased rapidly at first and reached 3.6×10^5 kPa at the displacement of 6.5 mm when the rotating band was fully pushed into the smooth forcing cone of barrel. During the displacement of the projectile of 6.5-24 mm, the pressure decreased suddenly and then increased slowly as the rotating band continued to be compressed in the smooth forcing cone portion of the barrel. The complicated change of the pressure curve in this period was due to the complex change of the stress state, the deformation of the rotating band, the change of the size of the cone into the barrel. When the rotating band entered the rifling (lands and grooves) of barrel, the pressure increased rapidly again and reached 5.4×10^5 kPa at 27.5 mm, indicating that the rotating band was entirely engraved into the grooves.

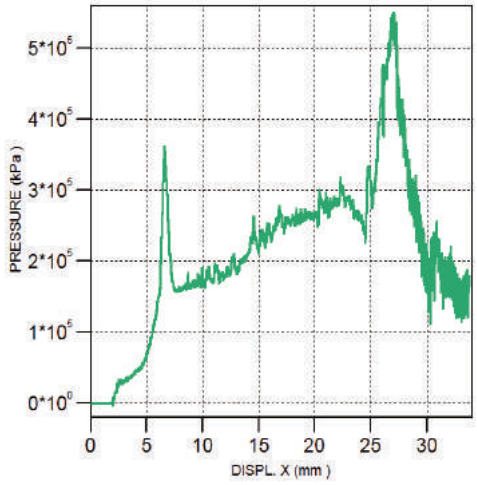

Fig. 15 Pressure of the barrel gun on the driving band

5 Conclusion

Based on the simulation results and semi-static experiment results on the process of rotating band engraving of 23 mm Armor-Piercing Incendiary Tracer Projectile when firing, the following conclusions have been drawn:

- the mechanism of the engraving process of the 23 mm armor piercing incendiary tracer projectile is a plastic deformation process of the rotating band material to fill the land and groove of the barrel. The rotating band material does not fail in the engraving process, and the mass of the rotating band is constant during the engraving process,
- after the rotating band engraving process, the projectile's velocity is 105 m s^{-1}, which is significantly different from the assumption used in the classical ballistic model,

- the simulation results show that the rotating band engraving time of the 23 mm armor piercing incendiary tracer projectile equals approximately 1.12 ms. The pressure of the barrel gun on the rotating band changes very complicatedly and the peak is achieved when the rotating band was entirely engraved into the grooves.

References

[1] CHURBANOV, E.V. *Internal Ballistics of the Boost Period* (in Russian). Saint Petersburg: Baltic State Technical University, 1997. ISBN 978-5-85546-117-6.

[2] VODOPYANOV, M.Ya. *Theory and Calculation of Artillery Projectile* (in Rusian). Saint Petersburg: Baltic State Technical University, 2002.

[3] DANILIN, G.A., V.P. OGORODNIKOV and A.B. ZAVOLOKHIN. *Basics of Small Arms Cartridge Design* (in Russian). Saint Petersburg: Baltic State Technical University, 2007. ISBN 978-5-85546-139-4.

[4] CARLUCCI, D.E. and S.S. JACOBSON. *Ballistics: Theory and Design of Guns and Ammunition.* 2nd ed. New York: CRC Press, 2013. ISBN 978-1-4665-6437-4.

[5] ANDREWS, T.D. Projectile Driving Band Interactions with Gun Barrels. *Journal of Pressure Vessel Technology*, 2006, **128**(2), pp. 273-278. DOI 10.1115/1.2172965.

[6] CARLUCCI, D., J. VEGA, M. POCOCK, S. EINSTEIN, C. GUYOTT and R. CHAPLIN. Novel Examination of Gun Bore Resistance Analysis and Experimental Validation. In: *Proceeding of the 23rd International Symposium on Ballistics* [online]. Tarragona: International Ballistics Society, 2007, pp. 313-320 [viewed 2021-11-14]. Available from: https://docplayer.net › 15587639-Novel-examination-of-gun-bore-resistance-analysis-and-experimental-validation.html

[7] TAO, C., Y. ZHANG, S. LI, C. JIA, Y. LI, X. ZHANG and Z. HE. Mechanism of Interior Ballistic Peak Phenomenon of Guns and Its Effects. *Journal of Applied Mechanics*, 2010, **77**(5), 051405. DOI 10.1115/1.4001561.

[8] WU, B., J. ZHENG, Q. TIAN, Z. ZOU, X. YU and K. ZHANG. Tribology of Rotating Band and Gun Barrel During Engraving Process under Quasi-Static and Dynamic Loading. *Friction*, 2014, **2**(4), pp. 330-342. DOI 10.1007/s40544-014-0061-3.

[9] SUDARSAN, N.V., R.B. SARSAR, S.K. DAS and S.D. NAIK. Prediction of Shot Start Pressure for Rifled Gun System. *Defence Science Journal*, 2018, **68**(2), pp. 144-149. DOI 10.14429/dsj.68.12247.

[10] *ANSYS Autodyn User's Manual* [online]. 2013 [viewed 2019-10-22]. Available from: https://vdocuments.net/ansys-autodyn-users-manual.html

[11] JIN Z.M. *Interior Ballistics of Guns* (in Chinese). Beijing: Beijing Institute of Technology Press, 2004.